ADVANCED ENERGY MATERIALS
www.advenergymat.de

Functionalized MXene/Halide Perovskite Heterojunctions for Perovskite Solar Cells Stable Under Real Outdoor Conditions

Masoud Karimipour, Ashitha Paingott Parambil, Kenedy Tabah Tanko, Tiankai Zhang, Feng Gao, and Monica Lira-Cantu**

Despite the performance improvement in perovskite solar cells (PSCs) when MXenes are employed as transport layers, device stability studies are still missing. Especially under real outdoor conditions where devices are subjected to the synergy of multiple stressors. In this work, functionalized 2D titanium carbide (Ti_3C_2) MXene is employed in normal PSC configuration, at the interface between the halide perovskite and the hole transport layer. The functionalization of the Ti_3C_2 MXene is made utilizing the same organic additive passivating the halide perovskite layer. The functionalizing strategy creates a continuous link between the MXene and the halide perovskite layer. Champion MXene-based PSCs revealed a ≈22% efficiency, in comparison with the control device showing 20.56%. Stability analyses under ISOS protocols under different conditions (dark, continuous light irradiation and real outdoor analysis) reveal that the enhancement of the PSCs lifespan is always observed when the MXene layer is employed. Analysis under continuous light irradaition (ISOS-L) reveal an almost 100% retention of the efficiency for the MXene-modified device, and outdoor testing (ISOS-O) carried out for > 600 h reveals a T_{80} of ≈600 h, while the control device degrades completely. To the best of the authors' knowledge, this is the first report of the stability assesment of MXene-based PSCs carried out under real outdoor (ISOS-O) conditions.

1. Introduction

2D MXene nanomaterials have been applied successfully in many fields of research such as sensors,[1] batteries,[2] supercapacitors,[3] water purification,[4] or energy harvesters[5–7] including many others. Among all types of 2D MXenes, Ti_3C_2-T_x nanosheets are characterized by their ease of chemical exfoliation, low cost, high conductivity, and abundant terminal groups for surface chemistry that permit the manipulation of its properties for the targeted applications.[8,9] The availability of abundant terminal groups on the surface of Ti_3C_2 nanosheets provides not only tremendous possibilities to chemically manipulate and harness its surface chemistry,[10] but also the feasibility of tuning its work function from metallic to semiconductor behavior.[11,12] The benefits of these properties have been also implemented in perovskite solar cells as selective or intermediate layers.[13–18] The main idea of applying 2D MXene nanosheets in perovskite solar cell has been mostly focused on addressing the issue of increasing the power conversion efficiency (PCE)[16,19,20] by means of defect passivation,[21] work function alignment[17,19,22] and efficient charge transfer.[5,13] For example, Bati et al. has employed a mixture of MXene nanosheets and single walled carbon nanotubes to passivate the electron transport layer (ETL :SnO_2 nanoparticle layer) at the perovskite interface with a demonstrated PCE over 20%.[23] Similarly, Wang et al., have also used MXene nanosheets as electron extracting booster on the SnO_2 NPs layer and observed a significant increase of the short current density (J_{SC}) due to the alignment of the work function studied by Ultraviolet photoelectron spectroscopy (UPS) and time-resolved photoluminescence (TRPL) analyses.[16] In a similar approach, MXene oxidation has been used as a novel strategy to enhance ETL/perovskite interface passivation by Yang et al.[24] and Niu et al.[25] Yang et al. found that the oxidation of MXene Ti_3C_2 can generate Ti—O bonds that lead to better attachment to perovskite film, thus the oxidized MXene can be used as ETL layer.[5] Niu et al. found that Nb_2C MXenes can be incorporated in the ilattice facets spacing of SnO_2 layer and

M. Karimipour, A. Paingott Parambil, K. Tabah Tanko, M. Lira-Cantu
Catalan Institute of Nanoscience and Nanotechnology (ICN2)
CSIC and the Barcelona Institute of Science and Technology (BIST)
Building ICN2
Campus UAB
Bellaterra, Barcelona E-08193, Spain
E-mail: masoud.karimipour@icn2.cat; monica.lira@icn2.cat
T. Zhang, F. Gao
Department of Physics, Chemistry and Biology (IFM)
Linköping University
Linköping 58183, Sweden

The ORCID identification number(s) for the author(s) of this article can be found under https://doi.org/10.1002/aenm.202301959

DOI: 10.1002/aenm.202301959

lead to the increase of SnO_2 grains and therefore better energy band alignment with the perovskite layer, increasing charge transfer.[25] In another report, MXene nanosheets have been added to the perovskite precursor solution and spin coated on substrates to obtain large grains after annealing, obtaining an enhanced PCE of the devices by increasing J_{SC}[13] or by passivating the Pb^{2+} and Pb^{I} antisite defects by extra etching of XMenes in HF-Dimethyformamide (DMF) solution, obtaining F-rich $Ti_3C_2T_x$ MXene nanosheets.[26] Recently, Agresti et al. have also investigated that the addition of MXene nanosheets in the bulk of the perovskite film together with the interface engineering of TiO_2/perovskite, would allow the fabrication of hysteresis-free devices with over 26% enhancement in PCE in comparison with the reference PCE.[19] Taotao Chen et al. also introduced Ti_3C_2 MXene nanosheets as accelerating hole extracting layer for all inorganic $CsPbBr_3$ perovskite solar cells (PCE 9.01%) together with a carbon contact. They found that MXene nanosheets can suppress electron recombination and enhance hole extraction at the interface of perovskite/carbon layers.[27] In another recent work, Yao et al. have incorporated graphene oxide (GO) into MXene nanosheet synthesis, to passivate further the oxygen and OH bonding of termination groups of MXene nanoshets and induce their hygroscopic behavior at the interface of carbon/perovskite layer to enhance charge extraction and achieved a significant PCE of 15.04% for $CsPbI_2Br$ carbon based solar cells.[28]

Reports on the application of MXenes for the stability enhancement of PSC have not been investigated profoundly. Most studies are limited to the analysis of devices under storage conditions in the dark. However, the study of accelerating aging tests under continuous light irradiation and especially under real outdoor operational conditions is currently in its infancy. Studies are reported mostly for inorganic perovskites which are known for their superior stability in comparison to the hybrid organic-inorganic perovskites. Among the few examples is the work developed by Chen et al. who has exposed inorganic perovskite solar cells to thermal and humidity conditions in the dark (ISOS-D-2 protocol).[29] In a similar way, Wang et al. have set encapsulated MXene-based PSCs devices under ambient air and ambient humidity conditions and tracked their shelf life in the dark (ISOS-D-2).[16] Analysis under continuous light irradiation (ISOS-L protocol) has been carried out by Song et al, who reported a 50% performance loss after 500 h in comparison with the control device that loses almost the 80% of its initial efficiency.[30] Hyuk Im et al., have recently reported the application of oxidized MXenes (OMXene) applied as a barrier layer for oxygen and moisture, in $CsPbI_3$ based PSC minimodules. The devices were stored in a chamber at 85°C/85 RH under light irradiation (no electrical connections) with Xenon lamp (modified ISOS-L3 protocol), resulting in device stability for more than 1000 h under continuous light irradiation.[31] Reports on the outdoor stability assessment of PSC can be found in the literature for 2D materials. For example, the groups of Kymakis and Di Carlo, et al.,[11] reported on the outdoor analysis of PSCs modules fabricated with 2D graphene and 2D MoS_2 carried out over months-long timescale.[11] However, to our knowledge, this is the first report of the stability assessment of 2D materials such as MXenes applied in PSCs and carried out under real outdoor (ISOS-O protocol) conditions.

In this work, functionalized 2D Ti_3C_2 MXene is employed in a normal PSC configuration and placed at the interface between the halide perovskite (HP) and the hole transport layer (HTL). The functionalization of the Ti_3C_2 MXene was made employing the same organic additive used for the halide perovskite film. Our strategy permits us to create an improved and continuous nexus between the MXene and the halide perovskite layer. Thermal admittance spectroscopy (TAS) analyses demonstrates that shalow defect passivation takes place when the functionalization is made only at the bulk of the materials, while both, shallow and deep defects, are passivated when an interface is involved. In addition, stability analyses under any analyzed condition (dark, continuous light irradiation and real outdoor analysis (ISOS-L and ISOS-O),[29] demonstrate that enhancement of the PSCs lifespan is always observed when the MXene layer is employed. Analysis under continuos light irradaition (ISOS-L) revealed an almost 100% retention of device performance, while outdoor testing (ISOS-O) for > 600 h revealed a T_{80} at ≈600 h, an oustanding response if compared to the control PSC with T_{80} at 250 h. To our knowledge, this is the first report of the stability analysis of MXene-based PSCs carried out under real outdoor (ISOS-O) conditions and indicates that MXene can pave the way to a highly stable PSC required for the commercialization of the technology.

2. Results and Discussion

2.1. MXene Delamination (d-MXene) and Functionalization with H3pp (MXene:H3pp)

The 2D MXene Ti_3C_2 was obtained commercially and used as received. The bulk MXene powder was delaminated using a method based on a multi-sequential solution stirring on Tetrapropylammonium hydroxide (TPAOH), Tetrabutylmmonium hydroxide (TBAOH), and Tetramethylammonium hydroxide (TMAOH) at room temperature for 24 h. The as-prepared dispersion was then washed three times in isopropanol following by centrifugation[7] (see Figure S1, Supporting Information). A green-colored dispersion was obtained as the characteristic of the delaminated MXene (d-MXene).

We have selected the additive 3-phosphonopropionic acid (H3pp) due to its two functional groups, phosphonate and carboxylate, and the outstanding device stability observed when applied within the halide perovskite layer.[32] In this case, we want to explore a possible beneficial effect of this type of additives when intercalated into the MXene layer. Thus, the functionalization of the MXene (MXene:H3pp) was obtained by the direct addition of the additive H3pp into the d-MXene dispersion and was sonicating for 20 min. The H3pp was employed using three different concentrations, 0,25 mg, 0.5 mg, and 1 mg, per 2 ml of green d-MXene. **Figure 1**a–d shows a schematic representation of the delamination (Figure 1b) and functionalization (Figure 1c) process followed by its deposition on a halide perovskite (HP) thin film (Figure 1d).

After synthesis, the structural, morphological, and electronic properties of the materials were verified comprehensively. Figure 1e shows the XRD of the d-MXene (red) and its comparison to the bulk MXene (blue) before delamination. The peaks indicated as (002), (006), (008), (103), and (110) correspond to

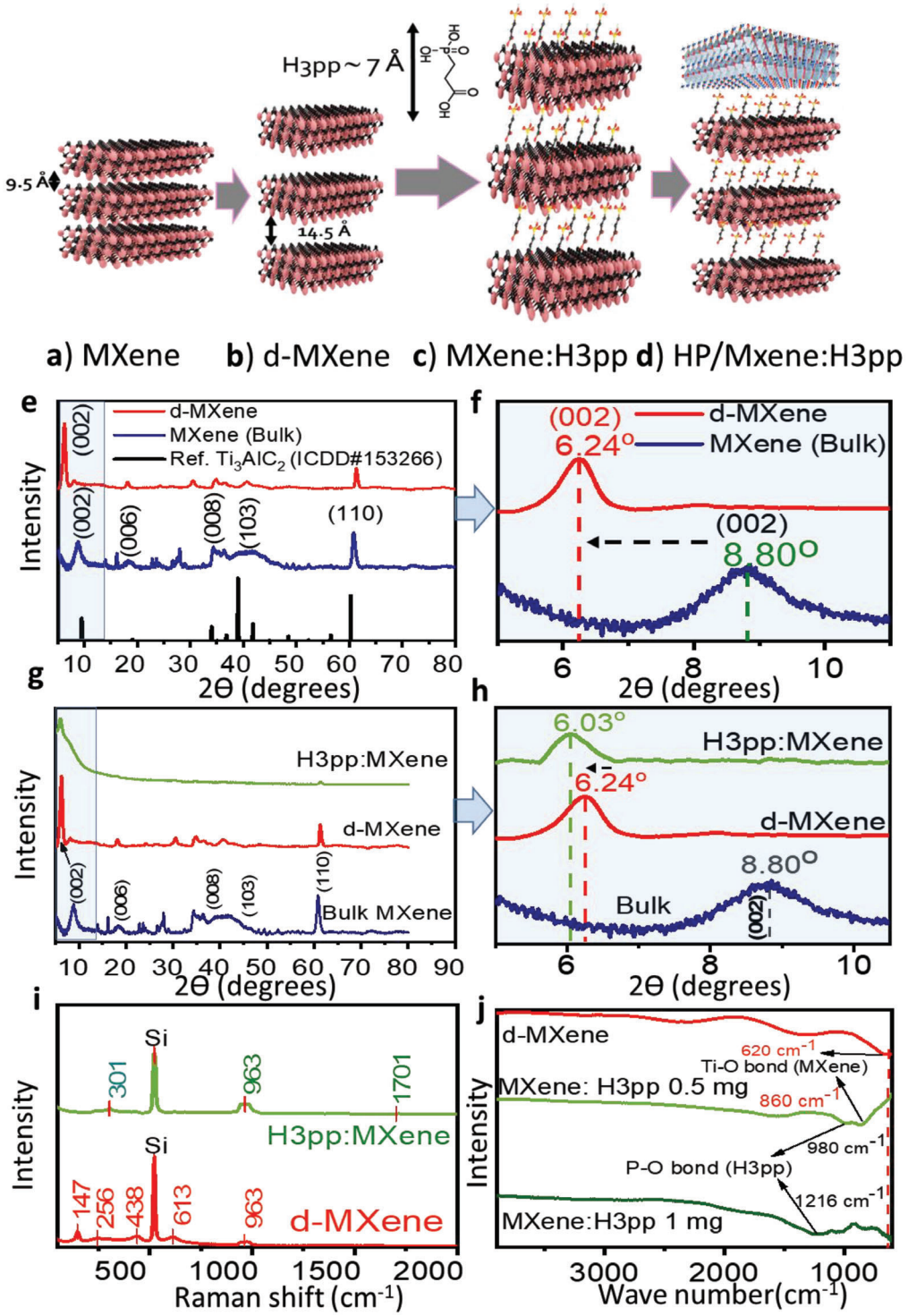

Figure 1. Schematic represenation of a) bulk MXene, b) delaminated MXene (d-MXene), c) MXene functionalized with H3pp (MXene:H3pp) and d) thre heterojunction made of the MXene:H3pp thin film and the Halide Perovskite thin film (MXene:H3pp/HP); (e) wide range X-ray diffraction (XRD) patterns of bulk MXene (blue), d-MXene and the pattern of the Ti_3AlC_2 ICSD No. 153 266[33–35]. as reference (black); f) zoomed area of e); g) wide range X-ray diffraction patterns of Bulk MXene (blue), d-MXene (red) and MXene:H3pp (green); (h) zoomed area of g); i) Raman spectra of d-MXene (red) and MXene:H3pp (green); j) Fourier-Transform inferared (FTIR) spectra of d-MXene (red) and MXene:H3pp functionalized with H3pp 0.5 mg (light green) and 1 mg (dark green).

Ti_3AlC_2 MAX phase, ICSD No. 153 266 (Figure 1e, black).[33–35] As it is inferred, the MXene structure undergoes a significant shift of the main diffraction peak (002) after delamination corresponding to an increase of lattice space in the (002) atomic plane direction. According to Figure 1e,f and the Bragg diffraction equation, this shift corresponds the expansion of the atomic plane from 10.01 Å to 14.14 Å. To scrutinize the effect of functionalization of MXene with the ligand H3pp, the XRD diffraction pattern of the MXene:H3pp is shown in Figure 1g and compared with the d-MXene before functionalization. Figure 1g,h show that the MXene functionalization causes a slight but observable shift of the (002) Bragg peak to lower angles, an indication of a slight increase of the atomic plane distance due to the intercalation of H3PP ligand (≈7.0 Å) within the MXene nanosheets (see schematic representation in Figure 1a–d). To examine, the ligand H3pp intercalation within the MXene nanosheets, Raman spectra of MXene:H3pp (MXene:H3pp) are shown in Figure 1i and compared with the d-MXene without ligand. Peaks at 127 cm^{-1}, 148 cm^{-1}, 245 cm^{-1}, 439 cm^{-1}, and 613 cm^{-1} correspond to different vibration modes of the Ti_3C_2 nanosheets in well agreement with the literature for the delaminated MXene (d-MXene).[36,37] The peak ≈245 cm^{-1} represents out-of-plane stretching vibration of surface Ti with —OH termination groups. After functionalization of the d-MXene with the H3pp molecule, the peaks at 148 cm^{-1}, 613 cm^{-1}, and 245 cm^{-1} have been quenched and a new peak at 301 cm^{-1} is observed which is attributed to the in-plane oxygen vibration modes from the termination groups (T_x) of MXene naosheets[38] while preserving the peak at 963 cm^{-1}.[37,39] These results demonstrate that after addition of the H3pp molecule, the Ti and C vibration modes are strongly weakened and the oxygen termination group are strengthened due to the presence of a P—O bonding in H3pp by its attachment to the MXene nanosheets surfaces.

We employed FTIR analyses to understand the type of bonding between the H3pp and the MXene nanosheets. Figure 1j shows the FTIR spectra of d-MXene and the MXene:H3pp functionalized with different amounts of H3pp (0.5 and 1 mg). The MXene:H3pp spectra shows representative peaks at 980 and 1216 cm^{-1} that are attributed to P—O vibration modes of the H3pp molecule.[40] With the increase of H3pp concentration during synthesis (from zero to 1 mg), the characteristic MXene vibration modes (Ti-O)[34] at 631 and 1317 cm^{-1} shifts toward higher wavenumbers (as shown with arrows in Figure 1j). This is an indication of the binding of the H3pp molecule to the MXene surface which provokes an increase of rigidity of the structure and vibration frequencies.[41] To further confirm the morphological properties of the materials, scanning electron microscopy (SEM) and transTEM images of the powdered samples are depicted in Figure S2 and S3, respectively (Supporting Information). We can observe the morphology evolution of the Ti_3C_2-T_x MXene from the bulk MXene to the delaminated MXene (d-MXene) and the functionalized material (MXene:H3pp). Once it evolves from the bulk to the delaminated MXene, a thin nanosheets with deflected surface can be observed attributed to structural distortion. Moreover, functionalization of d-MXenes with H3pp molecule, does not affects the morphology of the d-MXenes significantly by just slightly folding the edges of the nanosheets.

2.2. The Halide Perovskite (HP) and MXene:H3pp Heterojunction (HP/MXene:H3pp)

The fabrication of the HP/MXene:H3pp heterojunction was made by spin coating a solution of the MXene:H3pp on top of the $Rb_{0.05}Cs_{0.05}MA_{0.15}FA_{0.75}Pb(I_{0.95}Br_{0.05})_3$ quadruple perovskite thin film layer. The as-prepared HP/MXene:H3pp heterojunction was then annealed at 70°C for 3–5 min (see Figure S4, Supporting Information). Figure S5 (Supporting Information) shows the top view SEM images of the HP/MXene:H3pp heterojunction. For comparison purposes we included a HP/d-MXene thin film heterojunction (without the H3pp) and the control thin film made of the bare HP thin film. Figure S6 (Supporting Information) shows the EDX analyses of the d-MXene modified HP thin film corresponding to the SEM image of Figure S5 (Supporting Information). The samples show uniform coverage of the HP film with d-MXene nanosheets, and the observed MXene nanosheets are so thin that the HP grains are observable even thorough the MXene nanosheets. It also indicates the presence of large area MXene nanosheets for the Ti and Carbon elemental mapping, with distinctive contrast from the background, an indication of the presence of the MXene nanosheets on the surface of the perovskite film. To confirm the successful deposition of the MXene nanosheets without altering the HP thin film chemical composition, we carried out X-ray Photoelectron spectroscopy (XPS) analyses of the HP thin film with and without d-MXene on top (HP/d-MXene heterojunction) (Figure S7, Supporting Information). We observed that the deposition of d-MXene on the HP film, results in a slight increase of binding energy for Pb 4f, I 3d, and more importantly N1s orbitals which can alter the work function and effective passivation of the surface of the HP thin film.[42–44]

2.2.1. PSCs Applying the HP/MXene:H3pp Heterojunction as HTL

PSCs were fabricated in a normal configuration of the type: FTO/c-TiO_2/m-TiO_2/**HP/MXene:H3pp**/Spiro-OMeTAD/Au. Where the HP is the quadruple perovskite $Rb_{0.05}Cs_{0.05}MA_{0.15}FA_{0.75}Pb(I_{0.95}Br_{0.05})_3$ absorber, and the MXene:H3pp acts as the hole transport conductor. To understand the effect of the MXene nanosheets and its functionalization on the PV properties of the final device, we fabricated PSCs where the MXene:H3pp was replaced by the bare d-MXene and compared to the PSC without any interface modification (control). **Figure 2**a shows the schematic representation of a perovskite cell applying the functionalized MXene with H3pp (MXene:H3pp), at the interface between the SpiroOMeTAD and the HP layers. The photovoltaic (PV) response of the PSCs are depicted in Figure 2b–d, where Figure 2b shows the statistics observed for the PCE with the following values: control 19.45(±0.12) %, d-MXene 19.69(±0.11) %, and MXene:H3pp 19.82(±0.07) %. Figure 2c shows the reverse scan of the JV curves of the champion devices with highest PCE of 19.57 %, 19.80 %, and 19.89 %, for the control, the d-MXene and the MXene:H3pp devices, respectively. In general, the PV response is very similar for all devices, with a very slight increase in PCE observed for the solar cells applying the MXene:H3pp thin film. This enhancement mostly comes from a small increase in FF, V_{OC} and J_{SC}.[45,46] Incident photon to charge conversion

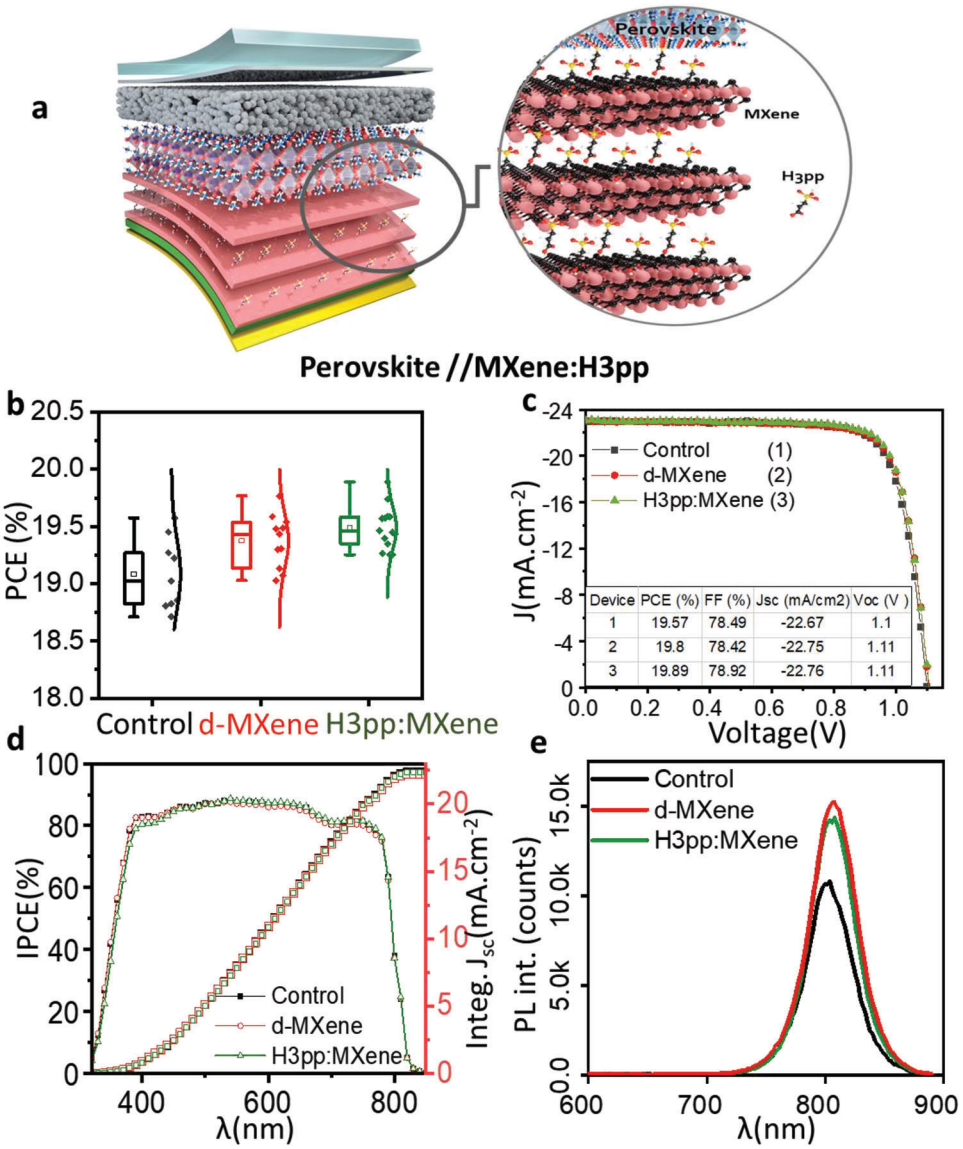

Figure 2. a) Schematic representation of a perovskite solar cell applying the MXene functionalized with H3pp (MXene:H3pp); b) PCE performance statistics of control PSC (black), PSC modified with d-MXene (red) and MXene:H3pp (green); c) JV curves of champion devices; d) IPCE of the champion devices; e) photoluminescence spectra (PL) of the HP film with/without a coated thin film of the d-MXene (red) and MXene:H3pp (green).

efficiency analyses (IPCE), Figure 2d, also agree with these results showing a slightly higher IPCE values for the solar cells employing the MXene:H3pp modified device. In addition, the calculated integrated J_{SC} values observed from IPCE analyses are in good agreement with those obtained from the JV curves. Figure 2e depicts the photoluminescence (PL) spectra of the different samples, where the HP/MXene:H3pp HP/d-MXene films (Figure 2e-green and red) changes both in terms of peak intensity and peak position with respect to the control sample (Figure 2e-black). Thus, the functionalization of the MXene with the H3pp ligand results in a slight but observable shift of the PL peak in ≈10 nm toward higher wavelengths (lower energies) together with an increase in the peak intensity. This shift could be due to bonding interaction of the MXene nanosheets with the HP surface as XPS analyses indicate. In summary, interface modification using both d-MXene and MXene:H3pp show enhancement in device performance parameters and effective charge extraction as well as initial indication of effective passivation of HP film.

2.2.2. The Interaction between the HP and the MXene:H3pp

The photovoltaic results and PL analyses described above indicate that the MXene functionalization may affect carrier redistribution in a PSC.[47] To prove this claim, we constructed the

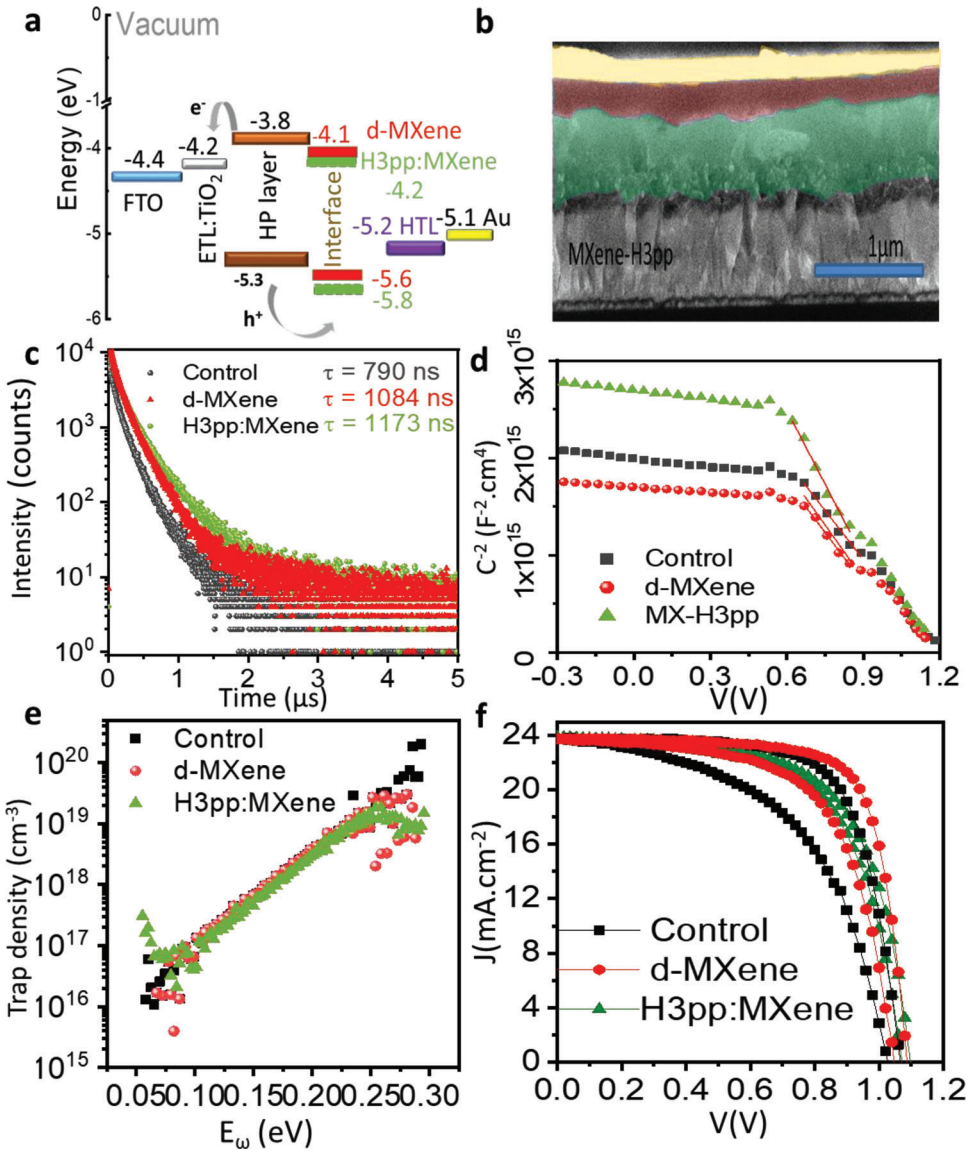

Figure 3. a) Band diagram of PSCs with/without interface modification using d-MXene (red) and MXene:H3pp (green) obtained from UPS analyses, b) TRPL spectra of the MHP films, c) Mott-Schottkey plots of the PSC devices with/without interface modification using d-MXene (red) and MXene:H3pp (green), d) Reverse-Forward JV scans of the devices, and e) trap density versus energy depth profile plots obtained from TAS analyses of the corresponding devices at 320 K.

energy band diagrams. For this, ultraviolet photoelectron spectroscopy (UPS) was performed (Figure S8, Supporting Information) to measure the work function and valence band position of the bare HP film (control) and the corresponding heterojunctions with the MXene thin films. The corresponding band diagrams are shown in **Figure 3**a (bandgap was calculated as 1.48 (±0.01) eV from IPCE measurements) for the corresponding device configuration with cross-SEM image in Figure 3b. The comparison of the band diagrams for the different samples indicates that the surface of the HP film, with an original work function (WF) of −4.51 eV for the non-modified film, experiences a shift downward to lower energies, −4.82 eV. Respectively, when the d-MXene is employed, a further decrease of the WF to −5.09 eV is observed when the MXene:H3pp (1 mg of H3pp) is used. In general, all the modifications indicate a shift of the VB from −5.29 eV for the control perovskite, to −5.67 eV for the d-MXene and −5.89 eV for the MXene:H3pp, an indication of an enhanced hole-extraction properties of the HP to the HTL, in agreement also with the IPCE analyses.

To further analyze the interaction between the HP and the MXene:H3pp, TRPL spectroscopy was performed on the devices and the resultant spectra are shown in Figure 3c. The calculated lifetime values, obtained by fitting with the three exponential decay function with the R^2>0.98 using pre-scripted PicoQuant software, show significantly larger values for samples employing delaminated MXene nanosheets in comparison with the control device. Moreover, PSCs with the MXene:H3pp thin film showed the longest lifetimes.

To analyze the possible defect passivation and non-radiative recombination on the HP surface by the d-MXene or MXene:H3pp thin films placed at the interface of the perovskite/HTL, we carried out density of trap states analyses. We employed capacitance measurements at different DC voltages at 20 kHz. Mott-Schottky analyses were performed, and the experimental details are described in Supporting Information (Section 4). The resulting Mott-Schottky plots are shown in Figure 3d and the calculated trap densities values are 3.49×10^{16}, 3.19×10^{16}, and 2.32×10^{16} $\frac{1}{cm^3}$ for the control, d-MXene, and MXene:H3pp devices, respectively.[48] The reduction of trap states observed for the MXene:H3pp device is more evident, while the d-MXene show a slight decrease in trap density value if compared to the control device. This is in well agreement with the results of TRPL analyses.[49] To shed more light on the trap densities and defect energy levels, a characterization of the distinct type of defects (deep or shallow trap states) was made. Thus, thermal admittance spectroscopy (TAS) was employed to study the significance of trap states in energy space for the modified and non-modified devices. Figure 3e shows the trap densities of the devices in energy space below conduction band that are calculated from TAS analyses at 320 K. The application of the d-MXene results in a 10-fold and 1000-fold decrease of the shallow and deep traps state, respectively, if compared to the control device. Interestingly, addition of H3pp as functionalized for d-MXene (MXene:H3pp) results in a 10-fold increase of shallow trap state if compared to the control device. This shift observed in the Fermi level toward the conduction band for the MXene-H3pp devices is in well agreement with the UPS results. Thus, the use of the Ti_3C_2 d-MXene as the interface between the HP and the Spiro-OMeTAD, works in favor of the passivation of both deep and shallow trap states of HP surface, while the introduction of the H3pp ligand in MXene:H3pp, results in the sole passivation of the deep trap states. These results are also in excellent agreement with the V_{oc} and hysteresis of the samples shown in Figure 3f, where an increase of the V_{oc} and the reduction of the hysteresis index is observed from the control device (bare HP), to the d-MXene and MXene:H3pp devices, respectively.

In summary, MXene nanosheets have been delaminated (d-MXene) and functionalized with the organic ligand H3pp (MXene:H3pp). The application of the functionalized MXene passivates both shallow and deep trap states. As a result, band alignment and charge extraction are improved.

2.2.3. Stability Assessment of PSCs Applying the HP/MXene:H3pp Heterojunction

In order to analyze the effect of the d-MXene and MXene:H3pp interface modifications on the lifetime stability of PSCs, we carried out stability assessment of compete solar cells following the ISOS-D, ISOS-L, and ISOS-O protocols.[29]

Stability under ISOS-D Protocol: The devices underwent an initial lifetime check under ISOS-D-1 protocol conditions by keeping the un-encapsulated samples in the dark and N_2 atmosphere (inside the glove box) for more than 3000 h, while JV curves were regularly measured during the whole test (**Figure 4**a–e). Figure 4a-d show the statistics of the PV parameters corresponding to the devices at their maximum PCE (day 25th of analysis) as observed in the ISOS-D-1 stability analysis shown in Figure 4e. We can observe in Figure 4a that at the 25th day of stability analyses, the PSC that maintain the best PV response is the one applying the MXene:H3pp sample (PCE of 19.85%), followed by the d-MXene (PCE of 19.59%) and finally the control device (PCE of 19.10%). At the end of the stability analysis (Figure 4e) the PSC applying the MXene:H3pp showed the highest stability (green), while the PSCs with the d-MXene (red) and the control device (black) were observed to maintain a similar but lower performance if compared to the former. This result is in good agreement with the interaction between the Ti_3C_2-T_x MXene and ligand molecules containing phosphonate groups, as in H3pp, which is a well know method to stabilize MXenes. The formation of a -Ti-O-P- bond (demonstrated by our Raman analyses) prevents the oxidation of MXene, improving the stability PSC of our devices.

Stability under ISOS-L Protocol: To further study the effect of MXene:H3pp and d-MXene nanosheets on the PSC stability under light irradiation conditions, the devices were set under simulated 1 Sun (calibrated LED lamp) and continuous N_2 gas flow at maximum power point tracking (MPPT) for 1000 h according to ISOS-L-1 protocol (Figure 4f). We observed that under these conditions, the most stable devices are those PSCs where MXene have been applied (d-MXene and MXene:H3pp). In this case, the d-MXene and the MXene:H3pp devices both show similar stability under continuous illumination and MPP conditions, always higher if compared to the control PSC. The d-MXene, MXene:H3pp, and control devices have reached T_{80} under MPP tracking at 256 h, 140 h, and 84 h, respectively.[50]

To investigate the effect of interface modification on the photostability of the MHP layer, the cross-section SEM images of the devices after 1000 h of MPPT under continuous light illumination (ISOS-L) were analyzed and are shown in Figure S9 (Supporting Information). The SEM images demonstrate that the control device has undergone perovskite degradation as indicated by the formation of large crystals (indicated as dotted circles) that have been attributed to the formation of PbI_2 ,[45] while d-MXene and MXene:H3pp devices do not show any sign of PbI_2 formation.[45] A clear formation of similar crystals as shown in Figure S9a (Supporting Information), for the control device can be seen in Figure S9b (Supporting Information) for the PSC applying only the H3pp at the interface between the HP and the Spiro-OMeTAD. The latter demonstrates that the application of MXenes (bare or functionalized) are beneficial for the stability of the PSC.

Stability under ISOS-O Protocol: Outdoor analysis is considered the best method to analyze the stability of PSCs due to the synergy of multiple stressors that vary in intensity and strength during the analysis of the PSCs under continous real conditions. Variations not only in light intensity but also in temperature, humidity, bias voltage, including the cycling of these factors, are observed during outdoor testing. In these conditions, the encapsulation made to the devices plays a critical role in the overall device performance. We have developed and protected a methodology for the encapsulation of our PSCs for outdoor analysis (Patent application submitted. Internal Reference Number ICN2IND_23-22) ensuring not only a good encapsulation but also the retention of the PV parameters before and after encapsulation (before outdoor analysis). Thus, PSCs with the highest PCE performances

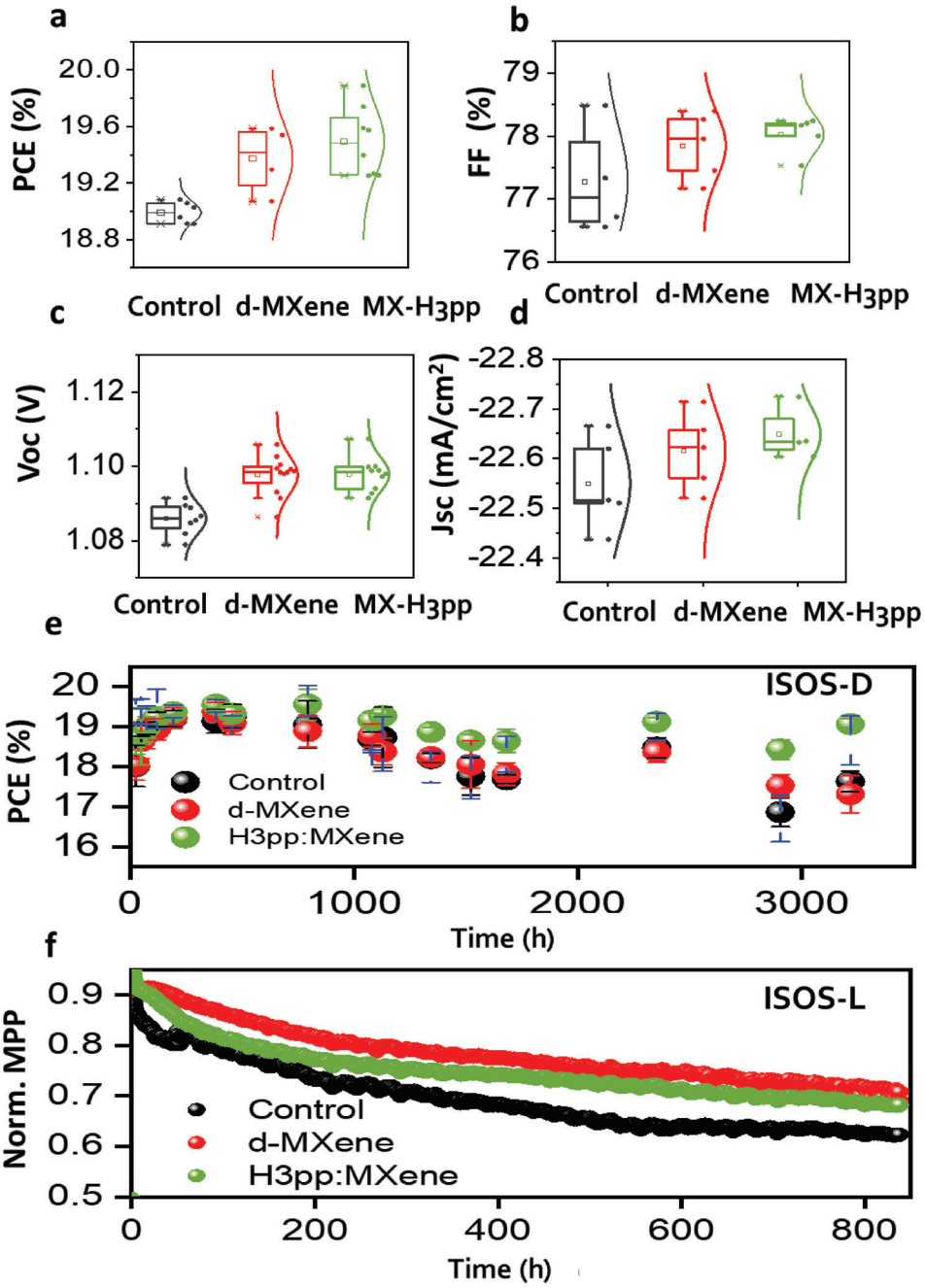

Figure 4. a–d) Summary of performance statistics of the devices at 25th day of life time tracking using ISOS-D-1 protocol (un-encapsulated, kept in dark, room temperature and N_2 atmosphere), e) life time tracking of the PCE of the devices for 2880 h (120 days) using ISOS-D-1 protocol, f) Normalized MPP tracking of the devices for 1000 h following ISOS-L-1 protocol (un-encapsulated devices, N2, under continuous simulated 1-sun light (A.M. 1.5G), at 20 °C).

observed before and after encapsulation (Figure S10, Supporting Information) were selected to be studied under outdoor conditions and MPP tracking (ISOS-O-1). **Figure 5a**,b shows the first 350 h of the outdoor stability analysis where only the data obtained at maximum PCE are plotted (Figure 5a) and all the data (day and night) are shown (Figure 5b) for the same test. In both cases, the temperature, humidity, power input (sun intensity illumination power) were also recorded alongside the measurements and are shown in Figure S11 (Supporting Information). We observed that the control PSC device (black) degraded completely after 275 h, while the PSCs applying the MXene:H3pp (green) together with d-MXene (red) have the best stability after 350 h. We selected four specific days at different times during the outdoor stability analysis to analyze in more detail the PV response. Figure 5c–f shows the evolution of the MPP for the whole day and night for each sample at ≈24 h, 90 h, 172 h,

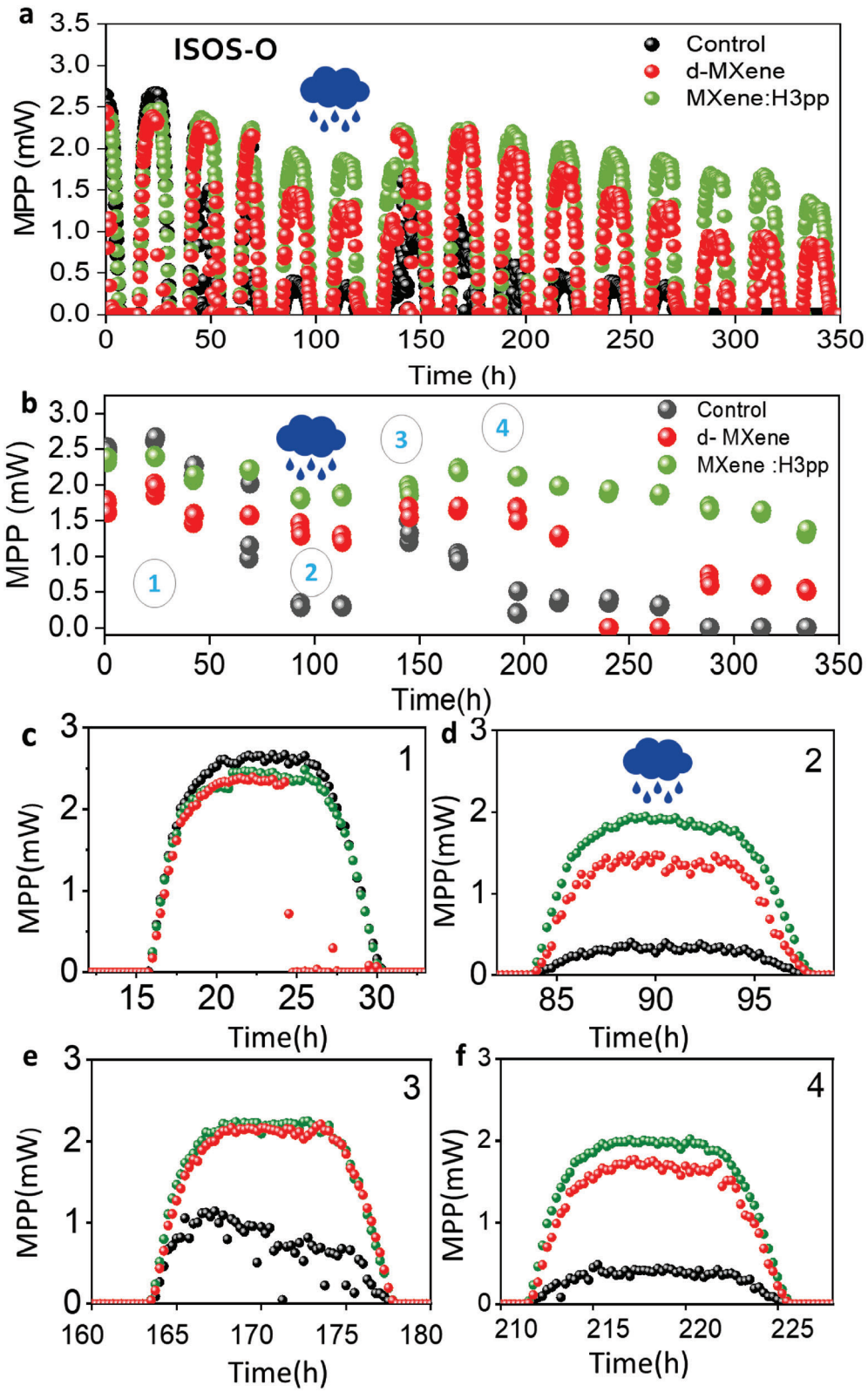

Figure 5. a) Obtained outdoor MPP values of the encapsulated devices (ISOS-O-1 at Barcelona, 41.5021° N, 2.1039° E, Spain) for 350 h fabricated by interface modification using d-MXene (red) and MXene:H3pp (green), b) The observed highest daily outdoor MPP values corresponding to highest irradiance for each day in (a) , c–f) selected days of MPP tracking of the devices for the comparison of performance evolution of the devices marked with numbers (1-4) in b).

and 218 h. We have observed that despite of the slightly better initial performance of the control device (day 1-Figure 5c), the PSC with the MXene:H3pp sample has superior performance under high humidity (60-85%) and low light intensities (90 h-172 h, Figure 5d,e), and it is able to maintain and even improve its performance after a low light irradiation and high humidity raining day (218 h, Figure 5f). An interesting observation is the recovery observed for the PSCs after the samples were exposed to a low-light irradiation and rainy day (after ≈115 h). The PSCs with MXenes recover and maintain their stability during the following days, while the control sample, although it also recovers initially, decays faster until complete degradation before 300 h. These results indicate that, in general, the use of a MXene as heterojunction with the HP enhances device stability, showing an outstanding response under continuous light irradiation (ISOS-L) when the H3pp functionalized MXene, MXene:H3pp, is employed. Thus, it can be concluded that the application of the functionalized Ti_3C_2 MXene with H3pp permits the effective defect passivation and the enhancement of the PSC device operational stability.[17,51] It is worth mentioning that although this interface modification does not increase the device efficiency significantly, it results in very stable devices, observed under both ISOS-L and ISOS-O protocols. Such a similar behavior has been reported also by Yakusheva et al.[22]

Summarizing the PSC stability analysis of the devices under ISOS-D (Dark), ISOS-L (continuous light irradiation) and ISOS-O (light-irradiation during day and recovery at night), we have observed that the best PSCs stability after 1000 h corresponds to the PSCs applying the MXene:H3pp in the dark, to the sole d-MXene under ISOS-L and to the MXene:H3pp under ISOS-O conditions. We attribute these different responses to several factors. Under dark conditions the H3pp additive prevents the degradation of the MXene through the formation of a strong Ti-O-P covalent bond, stabilizing the PSC. Under constant light irradiation we speculate that this response can be due to a photocatalytic effect of the MXene[52] which, under continuous light irradiation (ISOS-L, Figure 4f), the H3pp could be degraded by the MXene itself with time. However, under outdoor (ISOS-O, **Figure 6**a) the solar cells are subjected to variable stress factors such as light and temperature cycling or different light irradiation intensity. Some of these stressors are detrimental for the devices (like high light intensity) but others, like light cycling observed during day/night shifts, could be beneficial to the stability of perovskite solar cells due to the mechanism of recovery in the dark, well-known for PSCs. The multiple conditions observed under real outdoor conditions requires in-deep and careful experimental analysis and are currently being carried out in our laboratory.

2.3. The HP:H3pp/MXene:H3pp Heterojunction

Given that the use of MXenes and MXene:H3pp in PSCs resulted in an enhanced PV performance and device stability, we want to further improve these results by applying the organic additive H3pp also in the bulk of the HP. This methodology, the addition of additives with phosphonate and carboxylate groups within the halide perovskite layer, was developed by our group with excellent results in terms of device stability.[32] Thus, in this work, the H3pp molecule was added to the bulk of both, the MXene and the HP thin films, to form a HP:H3pp/MXene:H3pp heterojunction. The PSC configuration is the following: FTO/c-TiO_2/m-TiO_2/HP:H3pp/MXene:H3pp/Spiro-OMeTAD/Au. Where the HP is the quadruple perovskite $Rb_{0.05}Cs_{0.05}MA_{0.15}FA_{0.75}Pb(I_{0.95}Br_{0.05})_3$ absorber. The HP:H3pp precursor solution was prepared as detailed in Supporting Information (Section 1.5) and deposited by spin coating on top of the m-TiO_2 thin film. After drying, the MXene:H3pp was deposited on top of the HP:H3pp thin film following the method employed in the previous sections. For comparison purposes we also fabricated PSCs with only the HP/MXene:H3pp, and control PSC without any thin film modification.

2.3.1. Interaction with H3pp

Figure 6a shows a schematic representation of the PSC where the H3pp is part of the MXene layer and also part of the bulk of the HP. XRD measurements were carried out for the different samples (Figure 6b). We can observe that the thin films with the incorporation of MXene nanosheets show clearly less PbI_2 content and higher Bragg intensities for (002) preferential growth plane which indicates better crystallinity and possibly is due repair of edges at the crystal lattices explained by Hong et al.[47] Figure 6c,d show the TRPL and PL spectra of the different thin film samples. It can clearly be observed that the films employing the H3pp in both HP and MXene layers, have longer electron-hole recombination lifetime (1.180 μs). The PL spectra also indicates a red shift for both, the HP/MXene:H3pp thin film and the HP:H3pp/MXene:H3pp samples in comparison to the control HP thin film. According to Hong et al. this can be due to the effect of crystal change at the edges of the grains.[47] PSCs were fabricated with both the HP/MXene:H3pp and the HP:H3pp/MXene:H3pp heterojunctions and, for comparison purposes, we also included control PSCs devices where no modifications were made. Figure 6e shows statistics of the device PCEs, and Figure S12 (Supporting Information) contains the relevant statistical comparison of all the cells parameters for the different categories. Figure 6f shows the JV curves of the corresponding champion devices where the PCEs obtained are 21.21%, 20.9%, and 20.29% for HP:H3pp/MXene:H3pp, HP:H3pp/d-MXene, and the MXene:H3pp thin film as the interface, respectively. All the solar cells showed greater PCE than the control PSC with 20.28%. Figure S13 (Supporting Information) shows the IPCE of the champion devices for each sample in good correspondence with the J_{SC} values obtained by the corresponding integration.

2.3.2. Stability of the PSCs Applying the HP:H3pp/MXene:H3pp Heterojunction

Stability under Constant Light Irradiation Following ISOS-L Protocol: We carried out stability analysis of the different PSCs applying the ISOS-L-1 protocol under MPP tracking. Figure **7**a shows the change observed in maximum power point (MPP) for the first 1000 h under continuous simulated light irradiation of 1 sun at RT and under N_2 atmosphere. We observed that the best stability corresponds to the PSC employing the H3pp

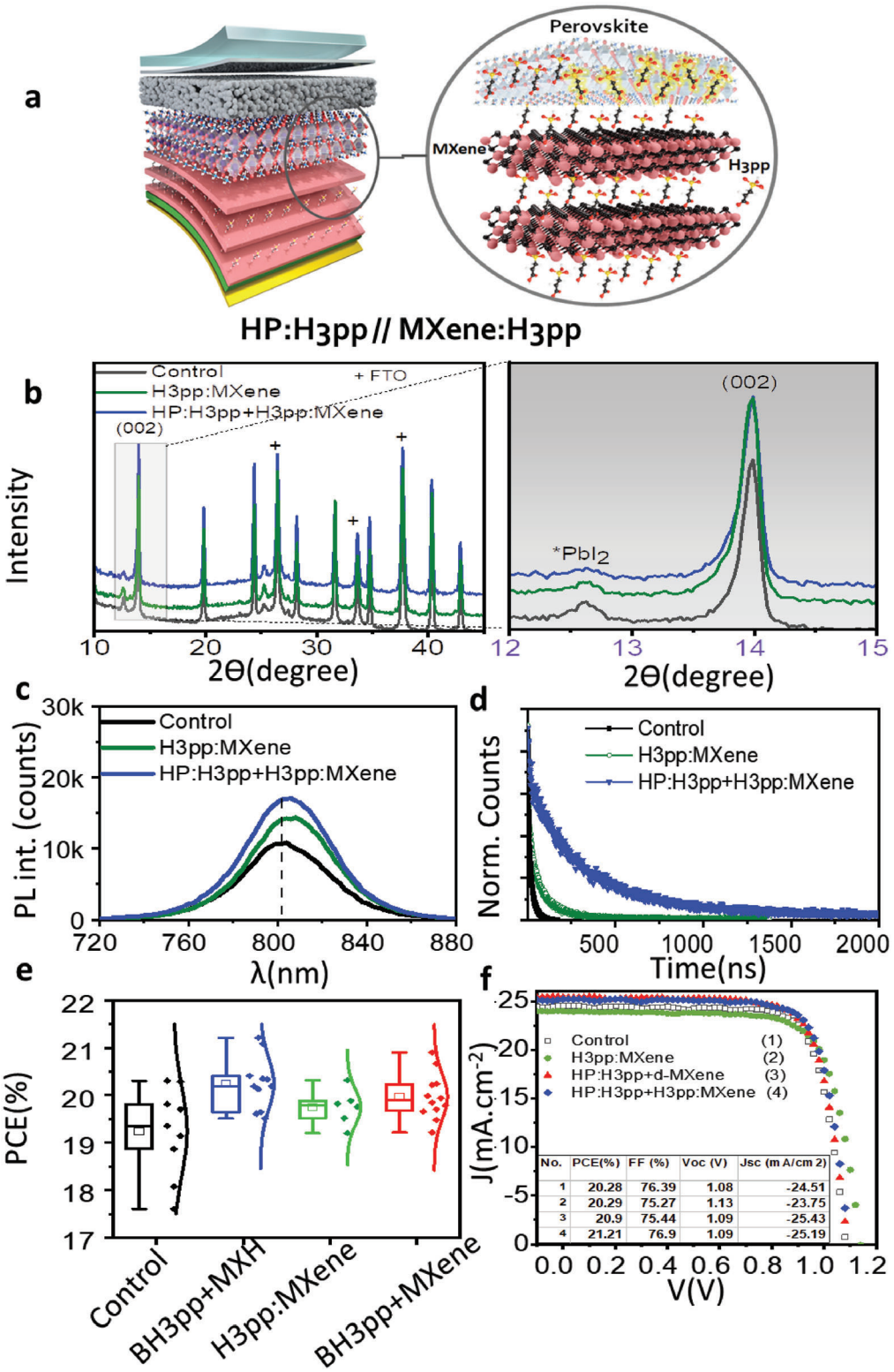

Figure 6. PSC employing the H3pp ligand in both the HTL and the absorber in PSC of the type: FTO/c-TiO_2/m-TiO_2/HP:H3pp/MXene:H3pp/Spiro-OMeTAD/Au. a) schematic representation of the PSC with the HP:H3pp/MXene:H3pp heterojunction. Characterization of the MXene:H3pp (green), HP:H3pp+d-MXene (red), the HP:H3pp/MXene:H3pp (blue) and the control PSC (black): b–d) XRD, TRPL and PL; e) PCE statistics, f) JV curves of the champion devices for each category with their relevant device parameters (inset table).

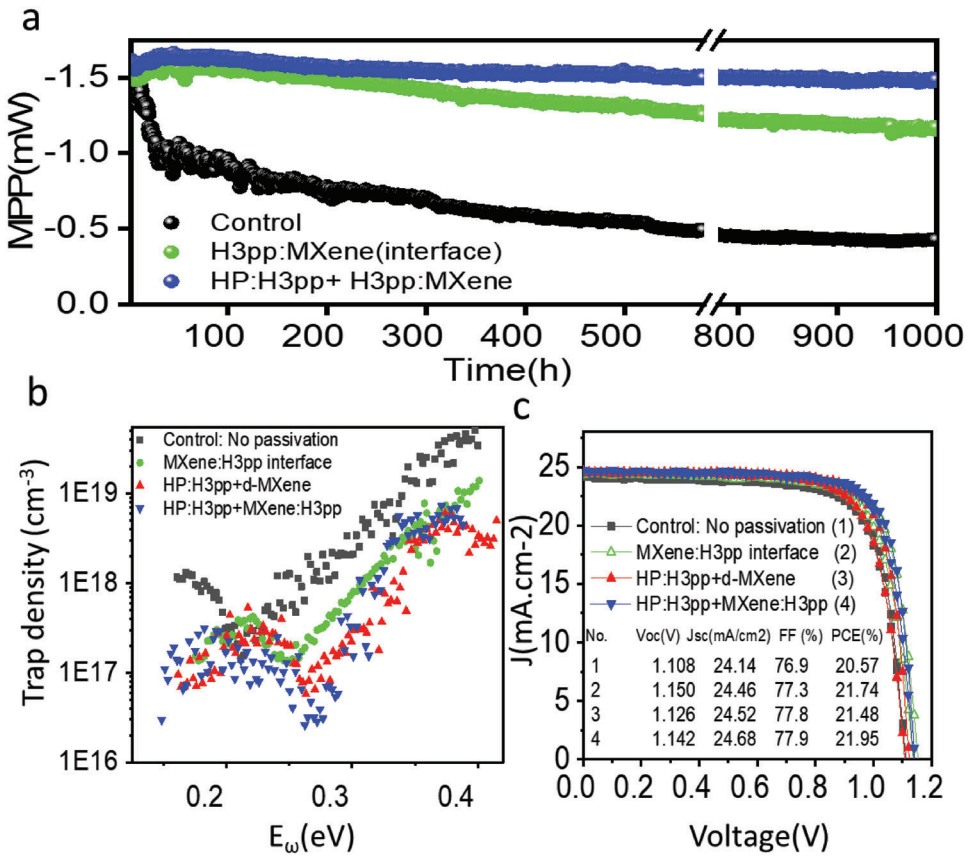

No.	Voc(V)	Jsc(mA/cm2)	FF (%)	PCE(%)
1	1.108	24.14	76.9	20.57
2	1.150	24.46	77.3	21.74
3	1.126	24.52	77.8	21.48
4	1.142	24.68	77.9	21.95

Figure 7. a) Stability analysis under MPP tracking of un-encapsulated devices following the ISOS-L-1 protocol (1sun, N_2 atmosphere and RT), and b) trap density versus energy depth profile from conduction band plots obtained from TAS analyses of the corresponding devices at 320 K, c) JV curves of champion devices with bulk and heterojunction passivation: Control with no passivation (black), Interface passivation with MXene:H3pp(green), bulk passivation with H3pp+ interface passivation with d-MXene (red) and, bulk passivation with H3pp+ interface passivation with MXene:H3pp abbreviated as HP:H3pp+MXene:H3pp (blue) including the table of device performance parameters under simulated 1-sun irradiance.

at both layers the perovskite (HP:H3pp) and the MXene (MXene:H3pp), showing almost no degradation for more than 1000 h at MPP (Figure 7a, red). The PSC applying the MXene:H3pp (Figure 7a, green) retained 75% of its initial MPP, in well reproducibility agreement with the results shown in Figure 4c. Both PSCs showed better stability than the control PSC (Figure 7a, black).

In view of the affomentioned findings, we conducted a TAS measurements for the selected high perfomance devices as shown in Figure 7b,c. Figure 7b depicts the trap density Vs. energy depth profile with respect to the conduction band edge. Our results clearly indicates that all the passivation works in favor of the reduction of trap state densities, from a 10 order of magnitude up to more than 100 times. The most significant trap reduction corresponds to the PSC where the additive is part of the bulk of both the MXene layer and the perovskite absorber which indicates a significant reduction of both shallow trap density and deep trap density of the order of 100 times for each one. Thus, it can be concluded that the passivation of only the bulk of the MXene or the perovskite, independently, passivates shallow trap densities[32] while the application of the H3pp in both layers and at the same time, passivates also the deep trap densities at the interface.

In summary, the outdoor stability results indicate that the simultaneously bulk and interface functionalization can lead to highly stable, durable devices. The use of organic additive molecules containing the phosphnate and carboxilate functional groups can be extended from the bulk to the interface and in combination with MXene nanosheets can act as ion migration inhibitor and moisture barrier, as well as effective trap density passivating agents. Figure 7c demonstrates the JV curves of the champion devices together with device performance parameters in Figure 7c-table inset. All PSC applying the H3pp molecule show higher PCE than the control device with 20.57% and 1.11 V, for PCE and V_{oc}, respectively. The corresponding values for HP:H3pp/MXene:H3pp device are 21.95%, and 1.14 V, respectively.

To demonstrate the effect of the H3pp ligand in the band diagram alignment of the PSC, UPS analyses of the different samples were carried out (see also Figure S14a, Supporting Information) and the corresponding band alignment is shown in Figure S14b (Supporting Information). The application of the H3pp in the MXene:H3pp and the HP:H3pp thin films is observed to decrease the VB position from −5.62 eV to −5.87 eV in comparison to the use of the H3pp only in the MXene:H3pp thin film. This can enhance the hole extraction and reduced electron

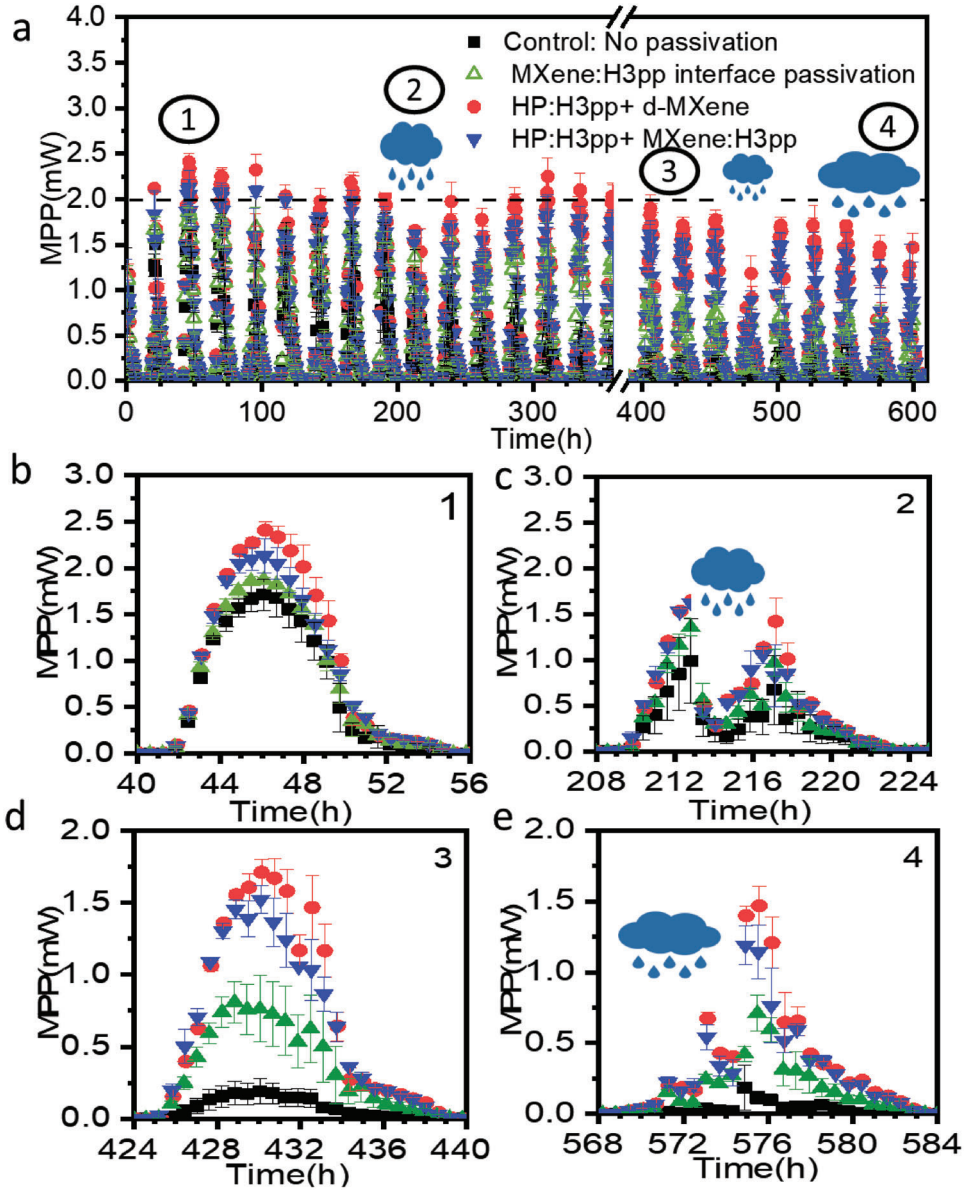

Figure 8. ISOS-O protocol tracking for PSCs employing bulk and interface passivation; a) obtained averaged MPP values for 3–4 devices for each category during 600 h by holding the encapsulated devices at their open circuit voltage and recording their JV by 20 min intervals in outdoor at Barcelona, 41.5021° N, 2.1039° E, Spain, b–e) Daily evolution of averaged MPP values for the different categories: Control with no passivation (black), Interface passivation with MXene:H3pp (green), bulk passivation with H3pp+interface passivation with d-MXene (red) and, bulk passivation with H3pp+ interface passivation with MXene:H3pp (blue) from 1–4, in different days of ISOS-O tracking.

recombination in the PSCs.[19] Chen et al. also reported the accelerated charge extraction via application of MXene nanosheets in all inorganic perovskite solar cells.[27] They concluded that the strong binding between = O surface bonds of Ti_3C_2 and undercordinated Pb atoms lead to passivation of interface and mitigation of work function alignment.[27] In summary, we have demonstrated that the simultaneous functionalization of the MXene transport layer and the HP absorber results in the best photovoltaic performance and excellent device stability under continuous light irradiation, ISOS-L protocol.

Stability under Outdoor Conditions Following ISOS-O Protocol: To scrutinize in more detail on the performance of the HP:H3pp/MXene:H3pp heterojunction in a PSC, we carried out an outdoor stability analyses for > 600 h by holding the devices at their open circuit voltage[53] and measuring their current-voltage (JV) every 20 min, see **Figure 8**. To ensure reproducibility, between 3 and 4 devices for each category were analyzed simultaneously, including the control PSC with no passivation (Figure 8a, black), the PSCs with the MXene:H3pp (Figure 8a, blue), the HP:H3pp/d-MXene (Figure 8a, red) and the HP:H3pp/MXene:H3pp (Figure 8a, green). Before the outdoor analysis, we verified that all PSCs efficiencies were between 18–21% under 1 sun simulated light intensity. Figure S15 (Supporting Information) shows the recorded humidity (black)

and sun light irradiance (red) for 600 h. Figure S16 (Supporting Information) demonstrates the collective obtained PCEs of all the devices per each category and Figure 8a shows the extracted and averaged (including error bars) MPP of each category.

Figure 8b–e show the daily evolution of MPP values for the four selected days. It can be elaborated from Figure S16 (Supporting Information) and Figure 8a (dashed lines are for a guide for the eye) that the control PSCs devices possess the most inferior stabilty with T_{80} between 250–275 h, while all the PSC employing MXenes (both the HP:H3pp/MXene:H3pp and the HP:H3pp/d-MXene, red and green respectively) show the highest stability with estimated T_{80} of 500 -600 h. Moreover, the PSCs devices with MXene:H3pp (blue color) show intermediate stability with an estimated T_{80} of 420–450 h (which is in good agreement with the results shown previosly in Figure 5a,b).

It is also worth noticing that daily tracking of the device´s performance show the stability of the devices under different light intensity, temperature and humidity conditions as shown in Figure 8b–e. Day (1) (Figure 8b, from 40 h -56 h) represents the MXene-based PSC photovoltaic response in a fully sunny day and at an early stage of the outdoor analysis. At this stage, the averaged MPP of the devices are very similar for all the categories, which is in good consistency with Figure 6f-table inset. This is also an indication of the consistency of our encapsulation process (Internal Reference Number ICN2IND_23-22).

The day labeled (2) (Figure 8c, from 208 h to 224 h) shows a low-light intensity and partially rainy day (see also Figure S15, Supporting Information). It is interesting to note that after the raining period, during the rise of the sunlight irradiance, all the PSCs employing the MXene material recover their photovotlaic performance while the control PSCs showed the worst recovery. The PSC devices employing the d-MXene nanosheets and the perovskite with the H3pp additive, showed the highest perfromance improvement.[32] These results are in agreement with the H3pp role of being a good linker to suppress ion migration in the bulk[32,53] and d-MXene as interface passivstor and humidity inhibitor.[30] During day labelled as (3) (Figure 8d, from 424 h to 440 h) after more than 400 h of holding the devices at their open circuit voltage, a clear distinction is observed between the PSCs applying the MXene and the control device, an indication of the beneficial effect of the simultaneously passivating the bulk of the perovskite with the H3pp ligand and the d-MXene nanosheets.

During day (4) (Figure 8e, from 568 h to 584 h), which was mostly a rainy and cloudy day (Figure S15), the beginning of the analyses shows low device performance. The later increase of the sun irradiance intensity, between 574 h -578 h, showed excellent recovery for the PSC when the MXene interlayer was employed.

In order to demonstrate any effect of hydrophobicity in our samples that could explain the enhanced stability of the solar cells, we carried out contact angle measurements of the the perovskite thin films with different functionalizations employing the pure H3pp, d-MXene and MXene:H3pp. Figure S17 (Supporting Information) shows the results of contact angle measurements. All modified samples show a slight increase in the contact angle of the water droplet independently of the presence of the H3pp or the MXene, with average values of 65.41 (±0.65)°, 64.87 (±0.27)°, 64.72°(±0.56)° for H3pp, d-MXene and MXene:H3pp respectively, versus 61.93 (±1.08)° value for the non-modified (control) perovskite film. These results clearly indicate that the superior performance of the interface modified devices are slightly influenced by hydrophobicity from the H3pp or the MXene. Thus, it can be inferred that the superior outdoor stability performance of the MXene modified devices with/without H3pp functionalization is largely due to interface deffect passivation, and ion migration suppression with small contribution of the hydrophobicity properties of the materials.[32]

In summary, the introduction of the H3pp within the halide perovskite absorber and the MXene HTL in the same PSC has shown the best stability response under continous light irradiation (ISOS-L) and under real oudoor conditions (ISOS-O). This response is attributed to the stability effect that the H3pp has on the MXene layer but also to the significant ion-inmobilization effect of the H3pp molecule when employed witin the perovskie layer. This ion-inmobilization effect has also shown to be beneficial for the recovery of the solar cells after outdoor periods under low light intensity or high humidity (clouds, rain) conditions. The solar cells employing the H3pp ligand are able to recover and stabilize after those conditions, while samples with only one of the layers contining the H3pp lighand or the control device, deteriorate steady with time until complete degradation. Contact angle measurements carried out to the samples supports our observation that the hydrophobic effect of the functionalizaed thin films don't play an important role on the device stability.

3. Conclusion

In summary, we demonstrate the application of functionalized 2D Ti_3C_2 MXene in Perovskite solar cells employed as the interface between the hole transport layer and the perovskite absorber. The functionalization of the Ti_3C_2 MXene was made employing the same organic additive chosen for the halide perovskite layer. Our strategy permits us to create an improved and continuous nexus between the MXene and the halide perovskite layers, including the interface. Defect passivation analyses by thermal admittance spectroscopy (TAS) indicates that shallow defects (responsible for device stability) are passivated at the bulk of the thin films, while deep defects (responsible for device efficiency) are also passivated at the interfaces. As a result, champion MXene-based PSCs with ≈22% efficiency were obtained, in comparisson with the 20.56% obtained for the control device. Stability analyses under any analyzed condition (dark, continuous light irradiation and real outdoor analysis) demonstrates that the enhancement of the PSCs lifespan is always observed when the MXene layer is employed. Especially relevant is the improvement in the device's lifespan observed under real operational outdoor conditions (ISOS-O) where the solar cells showed a T_{80} at ≈600 h. To our knowledge, this is the first report of the stability analysis of MXene-based PSCs carried out under outdoor (ISOS-O) conditions. Our results indicate that MXenes can pave the way towards highly stable perovskite solar cells. We believe our findings can have an enormous impact on perovskite solar cell stability, which is one of the main issues preventing the deployment of this photovoltaic technology.

Supporting Information

Supporting Information is available from the Wiley Online Library or from the author.

Acknowledgements

The authors give thanks to the Spanish State Research Agency for the grant Self-Power (PDI2022-143344OB-100 / AEI / 10.13039/501100011033). This work was part of the project PCI2020-112185, granted by MCIN/AEI/10.13039/501100011033 project and the European Union "NextGenerationEU"/PRTR. To the OrgEnergy Excelence Network (CTQ2016-81911-REDT), to the Agencia de Gestió d'Ajuts Universitaris i de Recerca (AGAUR) for the support to the consolidated Catalonia research group 2021 SGR 01617 and the Xarxa d'R+D+I Energy for Society (XRE4S). Part of this work was under Materials Science Ph.D. Degree for A.P. and K.T. of the Universitat Autonoma de Barcelona (UAB, Spain). ICN2 was supported by the Severo Ochoa program from Spanish MINECO (grant no. SEV-2017-0706) and was funded by the CERCA Programme/Generalitat de Catalunya. The ICN2 was supported by the Severo Ochoa Centres of Excellence programme, Grant CEX2021-001214-S, funded by MCIN/AEI/10.13039.501100011033. The authors thank the Spanish MINECO through the Severo Ochoa Centers of Excellence Program under grant no. SEV-2017-0706 for the postdoctoral contract to M.K. F.G. would like also to thank the supporting fund from the Swedish Energy Agency (P2022-00756).

Conflict of Interest

The authors declare no conflict of interest.

Data Availability Statement

The data that support the findings of this study are available from the corresponding author upon reasonable request.

Keywords

additive engineering, MXenes, passivation, perovskite solar cells, stability

Received: June 26, 2023
Revised: September 7, 2023
Published online: October 15, 2023

[1] G. P. Neupane, T. Yildirim, L. Zhang, Y. Lu, *Adv. Funct. Mater.* **2020**, *30*, 2005238.
[2] C. F. Du, X. Zhao, Z. Wang, H. Yu, Q. Ye, *Nanomaterials* **2021**, *11*, 166.
[3] S. Shah, M. Sayyad, K. Khan, J. Sun, Z. Guo, *Nanomaterials* **2021**, *11*, 2151.
[4] L. Damptey, B. N. Jaato, C. S. Ribeiro, S. Varagnolo, N. P. Power, V. Selvaraj, D. Dodoo-Arhin, R. V. Kumar, S. P. Sreenilayam, D. Brabazon, V. K. Thakur, S. Krishnamurthy, *Glob. Challenges* **2022**, *6*, 2100120.
[5] L. Yang, C. Dall'Agnese, Y. Dall'Agnese, G. Chen, Y. Gao, Y. Sanehira, A. K. Jena, X. F. Wang, Y. Gogotsi, T. Miyasaka, *Adv. Funct. Mater.* **2019**, *29*, 1905694.
[6] W. J. Sun, Y. Y. Zhao, X. F. Cheng, J. H. He, J. M. Lu, *ACS Appl. Mater. Interfaces* **2020**, *12*, 9865.
[7] S. Jolly, M. P. Paranthaman, M. Naguib, *Mater. Today Adv.* **2021**, *10*, 100139.
[8] L. Yin, C. Liu, C. Ding, C. Zhao, I. Z. Mitrovic, E. G. Lim, H. Wang, Y. Sun, Y. Han, Z. Li, L. Yang, C. Q. Ma, C. Zhao, *Cell Reports Phys. Sci.* **2022**, *3*, 100905.
[9] V. Natu, J. L. Hart, M. Sokol, H. Chiang, M. L. Taheri, M. W. Barsoum, *Angew. Chemie – Int. Ed.* **2019**, *58*, 12655.
[10] J. Ji, L. Zhao, Y. Shen, S. Liu, Y. Zhang, *FlatChem* **2019**, *17*, 100128.
[11] S. Pescetelli, A. Agresti, G. Viskadouros, S. Razza, K. Rogdakis, I. Kalogerakis, E. Spiliarotis, E. Leonardi, P. Mariani, L. Sorbello, M. Pierro, C. Cornaro, S. Bellani, L. Najafi, B. Martín-García, A. E. Del Rio, R. Castillo, M. Oropesa-Nuñez, S. Prato, M. L. Maranghi, A. Parisi, R. Sinicropi, F. Basosi, E. Bonaccorso, A. Kymakis, C. Di, *Nat. Energy* **2022**, *7*, 597.
[12] M. Mozafari, M. Soroush, *Mater. Adv.* **2021**, *2*, 7277.
[13] Z. Guo, L. Gao, Z. Xu, S. Teo, C. Zhang, Y. Kamata, S. Hayase, T. Ma, *Small* **2018**, *14*, 1802738.
[14] Y. Zhao, X. Zhang, X. Han, C. Hou, H. Wang, J. Qi, Y. Li, Q. Zhang, *Chem. Eng. J.* **2021**, *417*, 127912.
[15] Y. Li, Y. Lu, X. Huo, D. Wei, J. Meng, J. Dong, B. Qiao, S. Zhao, Z. Xu, D. Song, *RSC Adv.* **2021**, *11*, 15688.
[16] Y. Wang, P. Xiang, A. Ren, H. Lai, Z. Zhang, Z. Xuan, Z. Wan, J. Zhang, X. Hao, L. Wu, M. Sugiyama, U. Schwingenschlögl, C. Liu, Z. Tang, J. Wu, Z. Wang, D. Zhao, *ACS Appl. Mater. Interfaces* **2020**, *12*, 53973.
[17] D. Saranin, S. Pescetelli, A. Pazniak, D. Rossi, A. Liedl, A. Yakusheva, L. Luchnikov, D. Podgorny, P. Gostischev, S. Didenko, A. Tameev, D. Lizzit, M. Angelucci, R. Cimino, R. Larciprete, A. Agresti, A. Di Carlo, *Nano Energy* **2021**, 82.
[18] J. Ge, W. Li, X. He, H. Chen, W. Fang, X. Du, Y. Li, L. Zhao, *Mater. Today Energy* **2020**, *18*, 100562.
[19] A. Agresti, A. Pazniak, S. Pescetelli, A. Di Vito, D. Rossi, A. Pecchia, M. Auf der Maur, A. Liedl, R. Larciprete, D. V. Kuznetsov, D. Saranin, A. Di Carlo, *Nat. Mater.* **2019**, *18*, 1228.
[20] X. Chen, W. Xu, N. Ding, Y. Ji, G. Pan, J. Zhu, D. Zhou, Y. Wu, C. Chen, H. Song, *Adv. Funct. Mater.* **2020**, *30*, 2003295.
[21] V. S. N. Chava, P. S. Chandrasekhar, A. Gomez, L. Echegoyen, S. T. Sreenivasan, *ACS Appl. Energy Mater.* **2021**, *4*, 12137.
[22] A. Yakusheva, D. Saranin, D. Muratov, P. Gostishchev, H. Pazniak, A. Di Vito, T. S. Le, L. Luchnikov, A. Vasiliev, D. Podgorny, *Small* **2022**, *18*, 2201730.
[23] A. S. R. Bati, M. Hao, T. J. Macdonald, M. Batmunkh, Y. Yamauchi, L. Wang, J. G. Shapter, *Small* **2021**, *17*, 2101925.
[24] L. Yang, D. Kan, C. Dall'Agnese, Y. Dall'Agnese, B. Wang, A. K. Jena, Y. Wei, G. Chen, X. F. Wang, Y. Gogotsi, T. Miyasaka, *J. Mater. Chem. A* **2021**, *9*, 5016.
[25] Y. Niu, C. Tian, J. Gao, F. Fan, Y. Zhang, Y. Mi, X. Ouyang, L. Li, J. Li, S. Chen, *Nano Energy* **2021**, *89*, 106455.
[26] Y. Zhao, B. Li, C. Tian, X. Han, Y. Qiu, H. Xiong, K. Li, C. Hou, Y. Li, H. Wang, *Chem. Eng. J.* **2023**, 143862.
[27] T. Chen, G. Tong, E. Xu, H. Li, P. Li, Z. Zhu, J. Tang, Y. Qi, Y. Jiang, *J. Mater. Chem. A* **2019**, *7*, 20597.
[28] X. Yao, Z. Qi, P. Yang, J. Li, W. Yang, *Chem. Eng. J.* **2023**, 144315.
[29] M. V. Khenkin, E. A. Katz, A. Abate, G. Bardizza, J. J. Berry, C. Brabec, F. Brunetti, V. Bulović, Q. Burlingame, A. Di Carlo, R. Cheacharoen, Y. B. Cheng, A. Colsmann, S. Cros, K. Domanski, M. Dusza, C. J. Fell, S. R. Forrest, Y. Galagan, D. Di Girolamo, M. Grätzel, A. Hagfeldt, E. von Hauff, H. Hoppe, J. Kettle, H. Köbler, M. S. Leite, S. (Frank) Liu, Y. L. Loo, J. M. Luther, et al., *Nat. Energy* **2020**, *5*, 35.
[30] Y. Zhang, L. Xu, J. Sun, Y. Wu, Z. Kan, H. Zhang, L. Yang, B. Liu, B. Dong, X. Bai, *Adv. Energy Mater.* **2022**, *12*, 2201269.
[31] J. H. Heo, F. Zhang, J. K. Park, H. J. Lee, D. S. Lee, S. J. Heo, J. M. Luther, J. J. Berry, K. Zhu, S. H. Im, *Joule* **2022**, *6*, 1672.
[32] H. Xie, Z. Wang, Z. Chen, C. Pereyra, M. Pols, K. Gałkowski, M. Anaya, S. Fu, X. Jia, P. Tang, D. J. Kubicki, A. Agarwalla, H. S. Kim, D. Prochowicz, X. Borrisé, M. Bonn, C. Bao, X. Sun, S. M. Zakeeruddin, L. Emsley, J. Arbiol, F. Gao, F. Fu, H. I. Wang, K. J. Tielrooij, S. D.

Stranks, S. Tao, M. Grätzel, A. Hagfeldt, M. Lira-Cantu, *Joule* **2021**, *5*, 1246.
[33] W. Feng, H. Luo, S. Zeng, C. Chen, L. Deng, Y. Tan, X. Zhou, S. Peng, H. Zhang, *Mater. Chem. Front.* **2018**, *2*, 2320.
[34] Y. Li, X. Zhou, J. Wang, Q. Deng, M. Li, S. Du, Y. H. Han, J. Lee, Q. Huang, *RSC Adv.* **2017**, *7*, 24698.
[35] K. Chen, K. Yan, Q. Xie, H. Zhu, X. Li, Z. Dong, G. Yuan, J. Zhang, Y. Cong, *Res. Chem. Intermed.* **2022**, *48*, 4443.
[36] Y. Cao, Q. Deng, Z. Liu, D. Shen, T. Wang, Q. Huang, S. Du, N. Jiang, C. Te Lin, J. Yu, *RSC Adv.* **2017**, *7*, 20494.
[37] A. Sarycheva, Y. Gogotsi, *Chem. Mater.* **2020**, *32*, 3480.
[38] E. Berger, Z.-P. Lv, H.-P. Komsa, *J. Mater. Chem. C* **2023**, *11*, 1311.
[39] R. Botta, P. Chindaudon, P. Eiamchai, M. Horprathum, S. Limwichean, C. Chananonnawathorn, V. Patthanasettakul, A. Jomphoak, N. Nuntawong, *J. Raman Spectrosc.* **2019**, *50*, 1817.
[40] M. C. Zenobi, C. V. Luengo, M. J. Avena, E. H. Rueda, *Spectrochim. Acta – Part A Mol. Biomol. Spectrosc.* **2008**, *70*, 270.
[41] A. Barth, *Biochim. Biophys. Acta (BBA)-Bioenergetics* **2007**, *1767*, 1073.
[42] X. Jin, L. Yang, X.-F. Wang, *Nano-Micro Lett.* **2021**, *68*, 1.
[43] A. S. R. Bati, A. A. Sutanto, M. Hao, M. Batmunkh, Y. Yamauchi, L. Wang, Y. Wang, M. K. Nazeeruddin, J. G. Shapter, *Cell Reports Phys. Sci.* **2021**, *2*, 100598.
[44] C. Wu, W. Fang, Q. Cheng, J. Wan, R. Wen, Y. Wang, Y. Song, M. Li, *Angew. Chem., Int. Ed.* **2022**, *61*, e202210970.
[45] M. Karimipour, S. Khazraei, B. J. Kim, G. Boschloo, E. M. J. Johansson, *ACS Appl. Energy Mater.* **2021**, *4*, 14080.
[46] S. Cacovich, G. Vidon, M. Degani, M. Legrand, L. Gouda, J.-B. Puel, Y. Vaynzof, J.-F. Guillemoles, D. Ory, G. Grancini, *Nat. Commun.* **2022**, *13*, 2868.
[47] D. Hong, J. Li, S. Wan, I. G. Scheblykin, Y. Tian, *J. Phys. Chem. C* **2019**, *123*, 12521.
[48] H. Yang, Y. Shen, R. Zhang, Y. Wu, W. Chen, F. Yang, Q. Cheng, H. Chen, X. Ou, H. Yang, *Adv. Energy Mater.* **2022**, 2202207.
[49] E. V. Péan, S. Dimitrov, C. S. De Castro, M. L. Davies, *Phys. Chem. Chem. Phys.* **2020**, *22*, 28345.
[50] G. Yang, Z. Ren, K. Liu, M. Qin, W. Deng, H. Zhang, H. Wang, J. Liang, F. Ye, Q. Liang, *Nat. Photonics* **2021**, *15*, 681.
[51] C. Jiang, J. Zhou, H. Li, L. Tan, M. Li, W. Tress, L. Ding, M. Grätzel, C. Yi, *Nano-Micro Lett.* **2022**, *15*, 12.
[52] J. Zhu, E. Ha, G. Zhao, Y. Zhou, D. Huang, G. Yue, L. Hu, N. Sun, Y. Wang, L. Y. S. Lee, *Coord. Chem. Rev.* **2017**, *352*, 306.
[53] M. Prete, M. V. Khenkin, D. Glowienka, B. R. Patil, J. S. Lissau, I. Dogan, J. L. Hansen, T. Leißner, J. Fiutowski, H.-G. Rubahn, *ACS Appl. Energy Mater.* **2021**, *4*, 6562.